Experimental and computational investigation of benperidol and droperidol solid solutions in different crystal structures

*Kristaps Saršūns and Agris Bērziņš**

Faculty of Chemistry, University of Latvia, Jelgavas iela 1, Riga, LV-1004, Latvia

We explored solid solution formation between structurally highly similar active pharmaceutical ingredients droperidol and benperidol in different crystal phases formed by these compounds. We crystallized samples having different compound molar ratio to evaluate the solid solution formation capabilities. Different crystallization conditions were used to evaluate solid solution formation in different crystal phases, including nonsolvates, dihydrates, and several solvates. We also explored the phase obtained in the desolvation of the obtained solvated products. Our results clearly demonstrate that the formation of solid solutions strongly depends on the crystal structure, as in part of the structures almost complete replacement of benperidol with droperidol was achieved but in other structures the replacement was possible only up to a limited molar ratio. Moreover, only limited replacement of droperidol with benperidol was achieved and only in part of the structures. We investigated change of intramolecular and intermolecular energy introduced by the molecule replacement using computational calculations. We show that experimentally we obtained only structures where molecule replacement allows formation of efficient intermolecular interactions, and energetic requirements of intermolecular interaction changes to obtain solid solutions in nonsolvated phase are less strict than that for solvates.

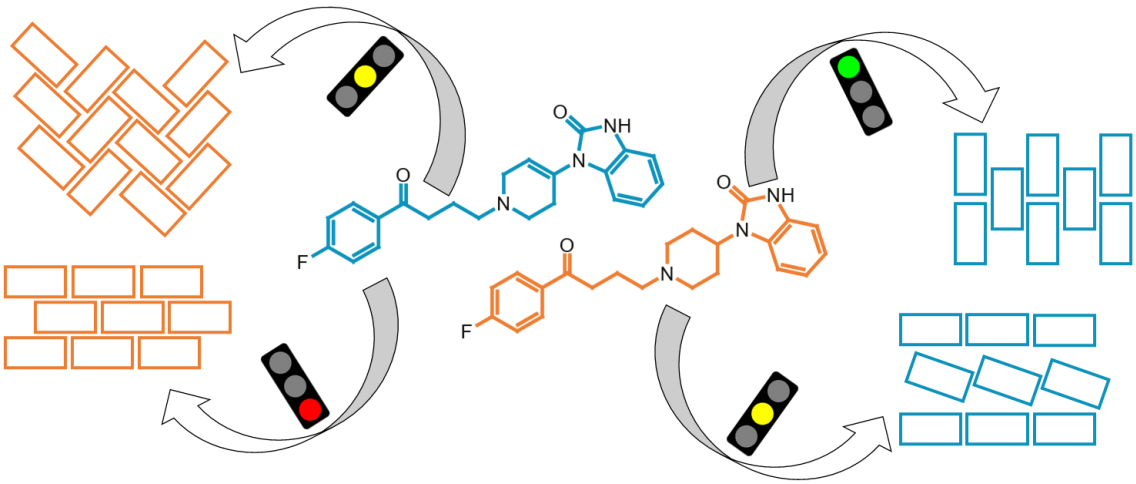

* Correspondence: agris.berzins@lu.lv; Tel.: +371-67672576

Experimental and computational investigation of benperidol and droperidol solid solutions in different crystal structures

*Kristaps Saršūns, Agris Bērziņš**

Faculty of Chemistry, University of Latvia, Jelgavas iela 1, Riga, LV-1004, Latvia

* Correspondence: agris.berzins@lu.lv; Tel.: +371-67672576

Abstract

We explored solid solution formation between structurally highly similar active pharmaceutical ingredients droperidol and benperidol in different crystal phases formed by these compounds. We crystallized samples having different compound molar ratio to evaluate the solid solution formation capabilities. Different crystallization conditions were used to evaluate solid solution formation in different crystal phases, including nonsolvates, dihydrates, and several solvates. We also explored the phase obtained in the desolvation of the obtained solvated products. Our results clearly demonstrate that the formation of solid solutions strongly depends on the crystal structure, as in part of the structures almost complete replacement of benperidol with droperidol was achieved but in other structures the replacement was possible only up to a limited molar ratio. Moreover, only limited replacement of droperidol with benperidol was achieved and only in part of the structures. We investigated change of intramolecular and intermolecular energy introduced by the molecule replacement using computational calculations. We show that experimentally we

obtained only structures where molecule replacement allows formation of efficient intermolecular interactions, and energetic requirements of intermolecular interaction changes to obtain solid solutions in nonsolvated phase are less strict than that for solvates.

1. Introduction

Crystal engineering includes developing of approaches and tools to use the already characterized crystals to predict formation of unknown crystal structures and their properties[1]. Approaches allowing prediction of formation of crystal structures of organic materials include evaluation of intermolecular interaction complementarity and preferences, with most specific being hydrogen bonds[2,3] and halogen bonds[4,5], and use of knowledge-based approaches. Knowledge-based approaches are often based on data in *Cambridge Structure Database (CSD)*, such as hydrogen-bond propensity[6–8] and non-bonded intermolecular interactions for a wide range of chemical groups available in *IsoStar* database[9] or use mining the *CSD* for more specific information[10–13]. Also, computational tools have been developed for predicting formation of specific phases[14–16] or crystal structures in general[17–19]. Crystal engineering approaches have been used to design and tune important physical properties of crystals, such as solubility[20,21], optical[22] and mechanical properties[23], melting point[24] etc.

Crystal engineering has been used to successfully design the strong intermolecular interactions in the solid state[8,25,26], but a belief that crystal structures can now be easily designed is overly optimistic, as often only the dominant supramolecular synthons are designed and part of the success lie in exploitation of limited number of functional groups having notably different properties[26–28]. For example, it has been shown[29,30] that in case of competing interactions, successful prediction is highly challenging or impossible. Moreover, weak intermolecular forces, their contribution to the stability of the crystal structure and effect of slight alteration of such forces

is even harder to be predicted and estimated[31–33]. However, polymorph structures often are a result of an interplay of weak intermolecular interactions and conformation, while strong interactions could be unaltered[34–36]. The rationalization of interactions in multi-component phases is often even more challenging, and the propensity of a compound to form solvates and co-crystals in general cannot be reliably predicted. Nevertheless, factors responsible for solvate formation for specific compounds have been identified[37–41], and there are strategies for prediction of formation of a multi-component phases for defined compounds[42–44].

Weak intermolecular forces are very important in formation of molecular solid solutions. The main requirement for formation of solid solution clearly is the miscibility of the components in the solid state[45]. This depends on two related concepts – structural mimicry[46,47] and crystal isomorphism[48,49]. It has long been demonstrated that primarily the size and shape of the entities have to be similar for a molecule replacement in the crystal lattice and formation of solid solution[50–52], provided the replacement do not break the intermolecular hydrogen bonding network and limitations regarding the dipole moment are followed[52]. The weak intermolecular forces, however, are often weak enough so that their alteration will not exclusively prevent formation of solid solutions, but important enough to determine the replacement possibilities[53]. Therefore, solid solutions between similar molecules are often formed only if the exchanged atoms or groups are not involved in directional or electrostatic interaction[45,53–56]. Overall, the studies of possibilities to replace relatively similar functional groups of organic molecules in formation of either isostructural phases[57] or solid solutions[58] has gained increased attention as tools to develop or test the rules of crystal engineering[59,60]. Moreover, solid solutions can be used to modify and fine tune various properties of crystals[48,61], including solubility[62,63], optical properties[64,65] etc.

In this study we explored the solid solution formation between two drug molecules: droperidol, 1-{1-[4-(4-fluorophenyl)-4-oxobutyl]-1,2,3,6-tetrahydro-4-pyridyl}-1,3-dihydro-2H-benzimidazol-2-one (Figure 1a), and benperidol, 1-{1-[4-(4-fluorophenyl)-4-oxobutyl]piperidin-4-yl}-1,3-dihydro-2H-benzimidazol-2-one (Figure 1b). Molecular structures of both compounds are very similar, and the difference is in the C8-C9 bond, which is saturated in benperidol and therefore is a part of a piperidine moiety, whereas unsaturated in droperidol and is a part of a 1,2,3,6-tetrahydropyridine moiety.

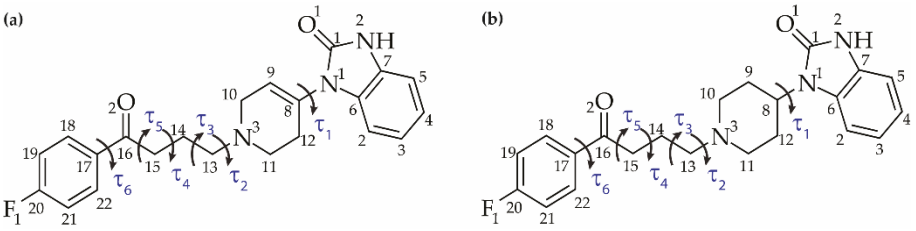

Figure 1. Molecular structure of (a) droperidol and (b) benperidol with the numbering of nonhydrogen atoms and labelling of flexible torsion angles.

The solid form landscape of both compounds has been explored[38,66]. Droperidol forms four polymorphs (in ambient crystallization **^{D}II** is obtained) and eleven solvates, including a set of isostructural solvates (among them methanol solvate **^{D}S$_{MeOH}$**, ethanol solvate **^{D}S$_{EtOH}$**, acetonitrile solvate **^{D}S$_{ACN}$** and nonstoichiometric hydrate **^{D}NSH**) and a dihydrate **^{D}DH**. Benperidol forms five polymorphs (in ambient crystallization **^{B}I** and **^{B}II** are obtained) and eleven solvates, including two sets of isostructural solvates (among them type 1 solvates with methanol **^{B}S$_{MeOH}$** and ethanol **^{B}S$_{EtOH}$** and type 2 solvate with acetonitrile **^{B}S$_{ACN}$**) and a dihydrate **^{B}DH**.

A possibility for formation of isostructural phases among these compounds has been studied by concluding that in conventional crystallization no isostructural phase between both compounds are obtained, but some are accessible via cross-seeding[57]. Unique structures for each of the compounds

are attributed to differences of the weak intermolecular interactions introduced by the molecular differences.

In this study the formation of solid solutions between droperidol and benperidol has been explored by comparing the formation of solid solutions in nonsolvated forms as well as in several solvates of these compounds. Computational calculations were performed to get an insight in the factors responsible for the differences of droperidol and benperidol solubility limits in several different phases formed by the other molecule and to evaluate the effects of intermolecular interactions in leading to the observed solubility differences.

2. Experimental section

2.1. Materials

Benperidol polymorph **^{B}I** (purity >99%) and droperidol polymorph **^{D}II** (purity >99%) were obtained from JSC Grindeks (Riga, Latvia). Organic solvents of analytical grade were purchased from commercial sources and used without further purification.

2.2. Crystal phase preparation

Solid solution (SS) formation was tested by recrystallization of benperidol and droperidol mixtures (in different ratios from 5 to 95 mol% benperidol). Nonsolvated droperidol and benperidol phases were prepared by dissolving a mixture of droperidol and benperidol in isopropanol at 70°C (obtaining nearly saturated solution) and rapidly cooling the solution to –5°C. Droperidol and benperidol dihydrate samples were obtained by dissolving a mixture of droperidol and benperidol in acetone at 50°C (obtaining nearly saturated solution) slowly adding a similar volume of water, and storing the resulting mixtures at 5°C. Droperidol and benperidol ethanol, methanol and acetonitrile solvates samples were obtained by dissolving a mixture of droperidol and benperidol in the respective solvent at 60-70°C (obtaining nearly saturated solution) and

rapidly cooling the solution to –5°C. More details of the crystallization experiments can be found in Table S1, Supporting Information.

The obtained solvated samples (containing either pure solid solution or a mixture of solid solutions in case of limited solubility) were desolvated by heating at 80°C (ethanol solvate and dihydrate samples) or 120°C (methanol and acetonitrile solvate samples) to test the phase obtained after the desolvation.

2.3. Powder x-ray diffraction (PXRD)

All of the obtained crystallization products were characterized by PXRD. The PXRD patterns were measured at ambient temperature on a *D8 Advance* (Bruker) diffractometer using copper radiation (CuK_α) at the wavelength of 1.54180 Å, equipped with a *LynxEye* position sensitive detector. The tube voltage and current were set to 40 kV and 40 mA. The divergence slit was set at 0.6 mm and the anti-scatter slit was set at 8.0 mm. The diffraction patterns were recorded using a 0.2 s/0.02° scanning speed from 3° to 35° on 2θ scale.

2.4. Differential scanning calorimetry/thermogravimetry (DSC/TG)

The differential scanning calorimetry/thermogravimetry (DSC/TG) analysis was performed with *TGA/DSC 2* (Mettler Toledo). Open 100 µL aluminum pans were used. Heating of the samples from 25 to 240°C was performed at a 10°C min^{-1} heating rate. Samples of 5 to 10 mg mass were used, and the nitrogen flow rate was 100 ± 10 mL min^{-1}.

2.5. Nuclear magnetic resonance (NMR) spectroscopy

^1H NMR spectra of pure benperidol and droperidol and most of the crystallization products dissolved in DMSO-d_6 were recorded at a nominal temperature of 300 K with a *Fourier 300 MHz* (*Bruker*) spectrometer. Chemical shifts (δ) were found in parts per million (ppm) using the residual solvent peak as an internal reference. For quantitative determination of each compound in the

mixture ^{1}H-NMR area of peaks at 10.82 (1H, s), 1.56 (2H, q) and 1.52 (2H, t) ppm were used for benperidol and at 10.90 (1H, s), 5.81 (1H, t) and 2.64 (2H, t) ppm for droperidol.

2.6. Theoretical calculations

Theoretical calculations were performed for three sets of crystal structures as in our previous study[67]. The first set (*Original*) was experimental crystal structures of droperidol and benperidol polymorphs and solvates, and included droperidol polymorph **^{D}II** GIXXOB[68], dihydrate **^{D}DH** DRPRDL[69] and solvates **^{D}S$_{EtOH}$** XOKKEP, **^{D}S$_{MeOH}$** XOKLAM and **^{D}S$_{ACN}$** XOKJUE[66] as well as benperidol polymorph **^{B}II** BENPRL02, dihydrate **^{B}DH** DUJPAB and solvates **^{B}S$_{EtOH}$** DUJXAJ, **^{B}S$_{MeOH}$** UHIZAO and **^{B}S$_{ACN}$** DUJXIR[70]. As the solvent molecules in **^{D}S$_{EtOH}$** and **^{D}S$_{MeOH}$** are disordered over two orientations related by inversion symmetry[66], the starting geometries of **^{D}S$_{EtOH}$** and **^{D}S$_{MeOH}$** without disorder were prepared in *P*1 symmetry by discarding one of the solvent molecule's orientation. The second set (*Isostructural*) was structures in which all the molecules of the original compound (e.g., benperidol) were replaced with molecules of the other compound (e.g., droperidol), see Figure 2. The third set (*Substituted*) was structures for which symmetry was removed, unit cell size was set to Z = 4 (Z = 6 for **^{B}II**) and one molecule of the original compound out of 4 (or out of 6 for **^{B}II**) was exchanged to the molecule of the other compound, see Figure 2. For droperidol **^{D}S$_{EtOH}$**, **^{D}S$_{MeOH}$**, and **^{D}S$_{ACN}$**, as well as benperidol **^{B}S$_{ACN}$** this meant doubling the unit cell volume, and for structures with Z'=2 or Z'=3 separate structures, designated with A, B and C, were obtained by substitution of each of the symmetrically unique molecule. In preparation of isostructural and substituted structures conversion of benperidol to droperidol always resulted in two sets of structures with different location of the double bound C8-C9. Among these two alternatives only the structure with the lowest energy after the geometry optimization in *Quantum ESPRESSO*, see below, was considered and analyzed.

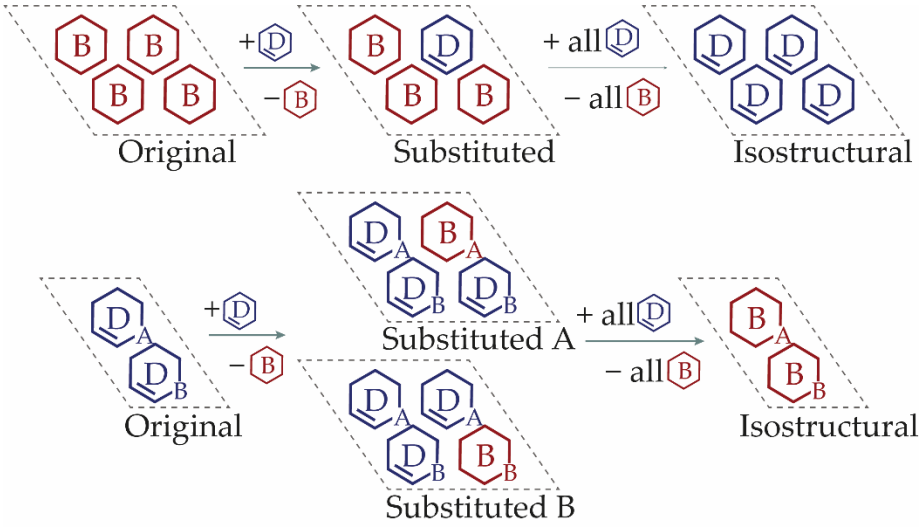

Figure 2. A schematic representation of construction of substituted and isostructural structures from the original structures used for the calculations. The upper part shows the construction of substituted and isostructural structures from an original benperidol structure, the lower part – construction of the two different possible substituted structures A and B involving doubling the unit cell size and the isostructural structure from an original droperidol structure with Z'=2.

Calculation of total cell energy and total intermolecular interaction energy of all the structures was performed using *Quantum ESPRESSO*[71] after relaxation of positions of all atoms and the unit cell parameters, with ultra-soft pseudopotentials from the original pseudopotential library and a 44 Ry plane-wave cut-off energy using PBE functional with vdW interactions treated according to the D2 method of Grimme[72]. The parameters of convergence, pseudopotentials and the k-point grid were used as suggested for structure optimizations of pharmaceutical molecules[73]. Energy of isolated molecules for calculation of total intermolecular interaction was calculated by extracting a single molecule from the optimized crystal structure and placing it inside a cubic unit cell with dimensions 40 × 40 × 40 Å. Total intermolecular interaction energy was calculated as the difference between the total cell energy and sum of all the energies of isolated molecules present in the unit cell.

Pairwise intermolecular interaction energy calculations for all the structures were performed in *CrystalExplorer 17.5* at the B3LYP/6-31G(d,p) level by calculating the pairwise interaction energies for molecules for which atoms are within 3.80 Å of the central molecule. Crystal structures were used after the geometry optimization in *Quantum ESPRESSO*.

The calculations of intramolecular energy were performed in *Gaussian 09*[74] at the M06-2X/6-31++G(d,p) level of theory. The potential energy surface scans of the flexible torsion angles[57] were used to determined the potential energy minimum conformations. These conformations were geometry optimized and energy of the global minimum was found for both molecules. Further benperidol and droperidol geometry was extracted from all the considered structures (after geometry optimization in *Quantum ESPRESSO*) and constrained geometry optimization was performed using *Gaussian 09* by freezing the torsion angles τ_1, τ_2 and τ_4 to the values as in the crystal structures. Intramolecular energy was calculated as the energy difference between the constrained and the global minimum geometry.

2.7. Crystal Structure Comparison and Analysis

Mercury 2020.2.0 software[75] was used for crystal structure visualization and analysis, including analysis and overlay of conformers present in the experimental and the modified crystal structures. Crystal structures after geometry optimization in *Quantum ESPRESSO* were used.

3. Results and discussion

As reported previously[57,66,70], the small differences of molecular structure of benperidol and droperidol alter the possibility of the central ring to form weak intermolecular interactions which is the reason why these two highly similar compounds form different crystal structures. Nevertheless, formation of a droperidol solvate $^{\text{D-iso-B}}\mathbf{S}_{\mathbf{EtOH}}$ isostructural to the benperidol solvate as well as $^{\text{D-iso-B}}\mathbf{DH}$ and $^{\text{D-iso-B}}\mathbf{II}$ in mixture with the original droperidol phases $^{\text{D}}\mathbf{DH}$ or $^{\text{D}}\mathbf{II}$ was

observed in the performed cross-seeding experiments[57]. The formation of such phases confirms that droperidol can crystallize in structures originally observed for benperidol, which suggests that also formation of solid solutions between these two compounds can be expected. Additionally, these results also suggest that the likelihood of the exchange of these molecules in the solid state depends on the crystal structure (exchange of benperidol with droperidol in the structure of ethanol solvate **$^{B}S_{EtOH}$** is the easiest, and it is also possible in structures of **^{B}DH** or **^{B}II**, whereas exchange of droperidol with benperidol was not observed).

In this study we explore the formation of solid solution as a tool to understand how easy one compound can replace the other one in the solid state and use computational calculations to identify the reasons for the different replacement capability in different crystal structures.

3.1. Experimental characterization of solid solution formation in different phases

Solid solutions obtained in crystallization

To evaluate the formation of solid solution between droperidol and benperidol in different phases we initially crystallized mixtures of both compounds in different ratios from solution. We used several different crystallization conditions to obtain different solid phases - nonsolvated forms (in the selected conditions polymorphs **^{B}I** or **^{B}II** could be obtained for benperidol and polymorph **^{D}II** for droperidol), dihydrates as well as ethanol, methanol and acetonitrile solvates. The crystallization conditions for preparation of these phases were chosen based on the already reported procedures for obtaining the respective single-component phases and solvates of these compounds[57].

The solid products obtained in the crystallization were characterized by PXRD and DSC/TG. The phases present in the samples were identified based on the agreement with the PXRD patterns of droperidol and benperidol polymorphs and solvates reported previously[66,70] and are given in

Table 1. The employed crystallization procedure always resulted in formation of the phase or phases with the desired composition, as nonsolvated phase or phases (**^{B}I**, **^{B}II** and **^{D}II**) were obtained from isopropanol, dihydrate or dihydrates (**^{B}DH** and **^{D}DH**) from acetone/water and the respective solvate or solvates from the organic solvents (**^{B}S$_{EtOH}$** and **^{D}S$_{EtOH}$** from ethanol, **^{B}S$_{MeOH}$** and **^{D}S$_{MeOH}$** from methanol and **^{B}S$_{ACN}$** and **^{D}S$_{ACN}$** from acetonitrile). In most of the cases crystallization of a mixture of droperidol and benperidol produced only a single phase, meaning that a solid solution (designated by **SS**) containing both components in the respective crystal structure formed, see Table 1. The benperidol : droperidol ratio in the obtained products was confirmed by recording ^{1}H NMR spectra of selected samples and always was close to the weighed ratio (see Supporting Information).

Table 1. Phases obtained in crystallization of a mixture of benperidol and droperidol for several selected molar ratios under conditions producing nonsolvates or the selected solvates. **SS** designates solid solution with crystal structure of the respective phase. Pure phases are in bold, phase mixtures are in italic.

Benperidol / mol%	Obtained phase				
	Nonsolvates	Ethanol solvate	Methanol solvate	Acetonitrile solvate	Dihydrate
0	**^{D}II**	**^{D}S$_{EtOH}$**	**^{D}S$_{MeOH}$**	**^{D}S$_{ACN}$**	**^{D}DH**
5	*^{D}II+SS^{B}II*	*^{D}S$_{EtOH}$+SS^{B}S$_{EtOH}$*	**SS^{D}S$_{MeOH}$**	**SS^{D}S$_{ACN}$**	**SS^{D}DH**
10	**SS^{B}II**	**SS^{B}S$_{EtOH}$**	**SS^{D}S$_{MeOH}$**	**SS^{D}S$_{ACN}$**	**SS^{D}DH**
20	**SS^{B}II**	**SS^{B}S$_{EtOH}$**	*SS^{D}S$_{Me}$+SS^{B}S$_{Me}$*	**SS^{D}S$_{ACN}$**	*SS^{D}DH+SS^{B}DH*
30	**SS^{B}II**	**SS^{B}S$_{EtOH}$**	*SS^{D}S$_{Me}$+SS^{B}S$_{Me}$*	*SS^{D}S$_{ACN}$+SS^{B}S$_{ACN}$*	*SS^{D}DH+SS^{B}DH*
40	**SS^{B}II**	**SS^{B}S$_{EtOH}$**	*SS^{D}S$_{Me}$+SS^{B}S$_{Me}$*	*SS^{D}S$_{ACN}$+SS^{B}S$_{ACN}$*	*SS^{D}DH+SS^{B}DH*
50	**SS^{B}II**	**SS^{B}S$_{EtOH}$**	**SS^{B}S$_{MeOH}$**	*SS^{D}S$_{ACN}$+SS^{B}S$_{ACN}$*	*SS^{D}DH+SS^{B}DH*
60	**SS^{B}II**	**SS^{B}S$_{EtOH}$**	**SS^{B}S$_{MeOH}$**	*SS^{D}S$_{ACN}$+SS^{B}S$_{ACN}$*	*SS^{D}DH+SS^{B}DH*
70	**SS^{B}II**	**SS^{B}S$_{EtOH}$**	**SS^{B}S$_{MeOH}$**	**SS^{B}S$_{ACN}$**	**SS^{B}DH**
80	**SS^{B}II**	**SS^{B}S$_{EtOH}$**	**SS^{B}S$_{MeOH}$**	**SS^{B}S$_{ACN}$**	**SS^{B}DH**
90	**SS^{B}II**	**SS^{B}S$_{EtOH}$**	**SS^{B}S$_{MeOH}$**	**SS^{B}S$_{ACN}$**	**SS^{B}DH**
100	**^{B}I**	**^{B}S$_{EtOH}$**	**^{B}S$_{MeOH}$**	**^{B}S$_{ACN}$**	**^{B}DH**

The results presented in Table 1 clearly show that the ability of replacing one molecule with the other strongly depends on the crystal structure, including even different capability to accommodate the other molecules by the isostructural solvate series $^{D}\mathbf{S}_{EtOH}$, $^{D}\mathbf{S}_{MeOH}$ and $^{D}\mathbf{S}_{ACN}$ and by $^{B}\mathbf{S}_{EtOH}$ and $^{B}\mathbf{S}_{MeOH}$. This appears both as different limit up to which the replacement is possible as well as even completely different ability of one molecule to replace the other. For example, no ability of benperidol to replace droperidol was detected in the nonsolvated phase $^{D}\mathbf{II}$ and the ethanol solvate $^{D}\mathbf{S}_{EtOH}$, whereas the replacement of benperidol with droperidol in ethanol solvate $^{B}\mathbf{S}_{EtOH}$ and nonsolvated phase $^{B}\mathbf{II}$ was achieved even up to a state close to a complete substitution, as solid solutions where 90% of the benperidol molecules were replaced were obtained, see PXRD patterns in Figure 3. These solid solutions are designated as $\mathbf{SS}^{B}\mathbf{S}_{EtOH}$ and $\mathbf{SS}^{B}\mathbf{II}$, respectively. These observations well match the results of the cross-seeding experiments performed previously[57], where a droperidol ethanol solvate $^{D\text{-}iso\text{-}B}\mathbf{S}_{EtOH}$ isostructural to the benperidol ethanol solvate was obtained in a pure form and formation of $^{D\text{-}iso\text{-}B}\mathbf{II}$ was also clearly observed. Therefore, it can be concluded that either fully isostructural structure $^{D\text{-}iso\text{-}B}\mathbf{S}_{EtOH}$ in which all of the benperidol molecules are replaced with droperidol exists and just was not obtained in the experimental conditions using 5 mol% benperidol, or instead of just seeding a solid solution containing a small amount of benperidol was actually obtained in the previously performed experiments[57].

Crystallization of pure benperidol from isopropanol in our performed experiments produced pure benperidol polymorph $^{B}\mathbf{I}$, even though very similar approach has been used[70] to prepare polymorph $^{B}\mathbf{II}$. Although when a small quantity of droperidol (5 mol%) was added $^{B}\mathbf{I}$ was still detected as the only crystallization product, ^{1}H NMR measurements (see Supporting Information) indicated that droperidol was present only in trace amount likely corresponding to impurity of droperidol phase not detectable by the PXRD method (Figure S10). This suggests that droperidol

apparently do not replace benperidol molecules in the structure of **^{B}I** in contrast to structure of **^{B}II** where almost complete replacement was achieved.

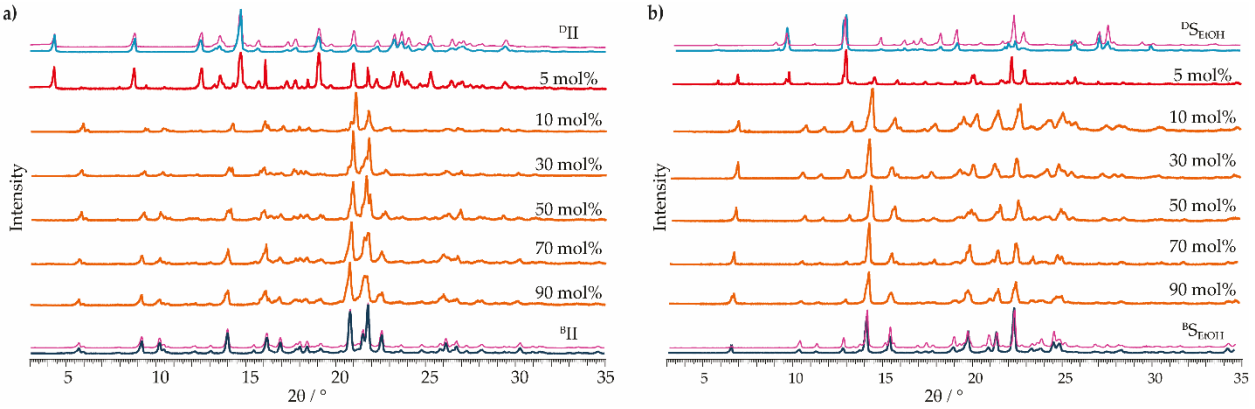

Figure 3. PXRD patterns of crystallization products when different ratio of benperidol and droperidol was crystallized from a) isopropanol by obtaining nonsolvated phase or phases and b) ethanol by obtaining ethanol solvate phase or phases. Labels show the weighted molar fraction of benperidol used in the crystallization. PXRD patterns for additional compositions are given in the Supporting Information. Solid solutions are in orange, phase mixtures in red, pure benperidol and droperidol phases in blue and patterns simulated from crystal structures in magenta.

Different outcome was observed for methanol and acetonitrile solvates and dihydrates. For these phases droperidol was able to replace benperidol molecules in the original benperidol phases **^{B}S$_{MeOH}$**, **^{B}S$_{ACN}$** and **^{B}DH** in a limited range up to 50 mol% or 70 mol% of benperidol depending on the particular solvated phase. Moreover, in contrast to the ethanol solvate and nonsolvated phases, in this case benperidol was able to replace droperidol molecules in the original droperidol phases **^{D}S$_{MeOH}$**, **^{D}S$_{ACN}$** and **^{D}DH** although only for relatively small benperidol contents up to 10 mol% for **^{D}S$_{MeOH}$** and **^{D}DH** and 20 mol% for **^{D}S$_{ACN}$**.

Characterization of the obtained solid solutions

All of the samples obtained in the crystallization were additionally characterized by DSC/TG analysis and solvated phases were desolvated, the obtained desolvation products were characterized using PXRD for phase identification and DSC/TG analysis for thermal characterization. More details on the characterization of the crystallization products are provided in the Supporting Information.

In all the DSC curves of nonsolvated solid solution **SS^{B}II** samples the melting endotherm is consistent with an essentially monophasic sample (see Figure 4). Across the composition range from 90 mol% down to 10 mol% benperidol, the onset and the peak temperature decrease monotonically as the amount of droperidol in the solid solution increase, consistent with the presence of a single solid solution phase in these samples, with the melting point between that of benperidol polymorph **^{B}II** ($T_{melt.}$ = 165°C) and droperidol polymorph **^{D}II** ($T_{melt.}$ = 151°C), see the phase diagram constructed from these data in Figure 4. A discontinuity in the melting behavior is observed for 5 mol% benperidol, as the sample contain a mixture of solid solution **SS^{B}II** and droperidol phase **^{D}II**.

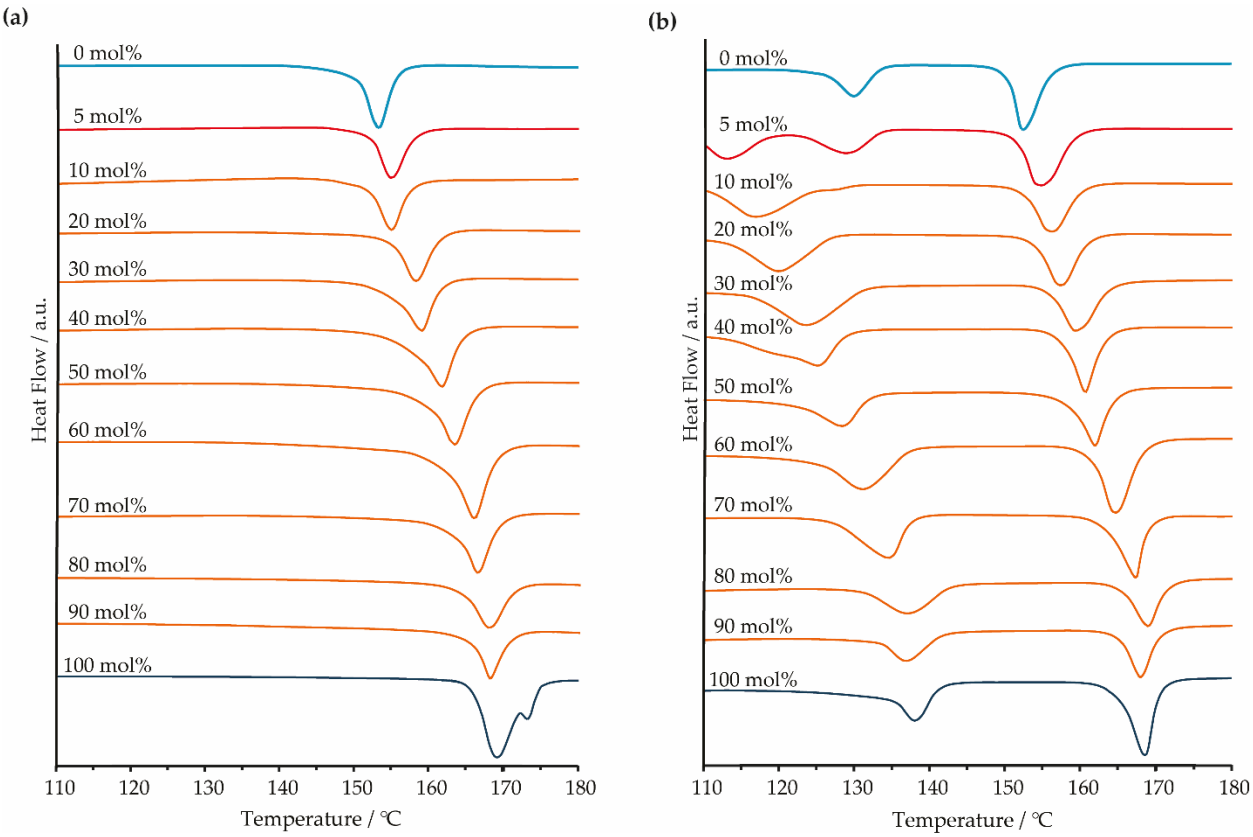

Figure 4. DSC curves for a) the nonsolvated solid solution **SS^{B}II** obtained in the crystallization from isopropanol, along with DSC curves of droperidol **^{D}II** and benperidol **^{B}II** and b) the solvated solid solution **SS^{B}S$_{EtOH}$** obtained in the crystallization from ethanol along with DSC curves of droperidol ethanol solvate **^{D}S$_{EtOH}$** and benperidol ethanol solvate **^{B}S$_{EtOH}$**. The labels represent the benperidol content used in the crystallization. Solid solutions are in orange, phase mixtures in red and pure benperidol and droperidol phases in blue.

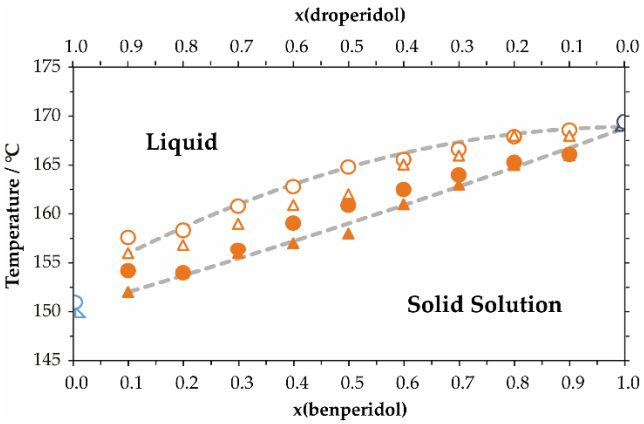

Figure 5. Part of a melt phase diagram of benperidol-droperidol binary system obtained from the DSC measurements. The circles correspond to data from samples obtained in the crystallization from isopropanol and were used to construct the phase diagram, in which the lines are guides for the eyes. The triangles correspond to the data measured for samples obtained in the desolvation of ethanol solvate samples and illustrate the agreement with the thermal characteristics of samples obtained in the crystallization.

The DSC curves of the solvated solid solution $\mathbf{SS^{B}S_{EtOH}}$ showed that a single desolvation peak is present across the composition range starting from pure benperidol to 10 mol% benperidol, and the desolvation temperature decreases monotonically as the amount of droperidol in the solid solution increases, consistent with the presence of a single solid solution phase in these samples. In contrast, two desolvation peaks are present for sample with 5 mol% benperidol, which agrees with the presence of two solvated phases. Similar monotonic decrease of the desolvation temperature by increasing the amount of droperidol in the solid solution was observed also for the solvated solid solution $\mathbf{SS^{B}S_{MeOH}}$, and a tendency for the desolvation temperature to decrease by increasing the amount of the compound replacing the original compound was observed also for other solvated solid solutions. Besides, the melting peak of the obtained desolvation product of $\mathbf{SS^{B}S_{EtOH}}$ and in most cases also that obtained from the other solvated samples decreased

monotonically over the whole composition range by increasing the amount of droperidol in the sample. To fully understand this monotonic decrease over the whole composition range, solvated samples obtained in the crystallization were desolvated and characterized.

By heating the solvated samples obtained in the crystallization experiments a desolvated product always formed prior to the physical melting of the sample. Interestingly, we observed that the desolvation product is not dependent on the phase composition of the solvated sample being desolvated. The desolvation product of the only solvated solid solution existing in nearly the whole composition range, **SS^{B}S$_{EtOH}$**, always was the nonsolvated solid solution **SS^{B}II**. This is consistent with the main desolvation product of pure benperidol ethanol solvate **^{B}S$_{EtOH}$** being polymorph **^{B}II**[70]. Moreover, the nonsolvated solid solution **SS^{B}II** was obtained as the only desolvation product also by desolvating all the samples obtained from methanol, acetonitrile, and acetone/water regardless of whether the sample contained solid solution having structure of the original benperidol solvate, solid solution having structure of the original droperidol solvate or even the mixture thereof. This was confirmed both by the PXRD patterns of the desolvated samples as well as by their DSC curves in which the melting endotherm was consistent with an essentially monophasic sample with the melting onset and peak temperatures matching that of **SS^{B}II** having identical component composition. The formation of **SS^{B}II** in the desolvation of phase mixture is also consistent with already reported formation of phase isostructural to **^{B}II** in desolvation of a mixture of **^{D}DH** and **$^{D\text{-}iso\text{-}B}$DH** obtained in the cross seeding experiments[57] and suggest that in those experiments **$^{D\text{-}iso\text{-}B}$DH** must have actually been **SS^{B}DH** containing some benperidol from the used seed material.

Considering the desolvation process, this means that the desolvation of all of the solvates should be associated with a recrystallization of the sample and is not a simple structure rearrangement

after the solvent loss[76,77], which could not lead to a formation of a single solid solution phase **SS^{B}II** regardless of the phase or phases present in the solvated sample.

In general, the formation of solid solution **SS^{B}II** both in crystallization and desolvation experiments as the only nonsolvated crystal structure in cases when both benperidol and droperidol are present indicates on its superior stability compared to any other nonsolvated binary phase or even a mixture of benperidol and droperidol single component phases.

3.2. Structural and computational characterization of solid solutions

Detailed comparison of the crystal structures of benperidol and droperidol by focusing on the reasons for formation of different crystal structures and comparison of the experimental structures with those of mostly hypothetical isostructural phases is already available[57]. In this study, however, we focus on evaluation of structural and energy related aspects for formation of solid solutions by replacing part of the original molecules in the crystal structure with the molecules of the second compound. **^{B}I** was not considered, as the solid solution formed in benperidol structure **^{B}II**, and part of the computational calculations were not possible for **^{B}I** because of the large size (Z=18) of its unit cell.

Comparison of molecular conformation

A comparison of the crystal structures of benperidol and droperidol nonsolvates and solvates show that only for a pair of nonsolvates **^{B}II** - **^{D}II** and acetonitrile solvates the same hydrogen bonding motif is present, whereas in all the other cases (most pairs of identical solvates, including dihydrates, where chains differ with hydrogen bonding) it is different (see Table 2). Comparison of droperidol and benperidol conformation showed that conformation in nonsolvates are notably different (with benperidol **^{B}II** having the most distinct conformation), whereas the conformation in the studied solvates is similar. Even though this analysis shows that the replacement of

molecules in nonsolvates would require notable adaptation of conformation, the resulting conformation still would correspond to low energy region of the PES[57].

Table 2. The basic crystal structure information of selected benperidol and droperidol phases, by comparing structures of benperidol and droperidol nonsolvates and solvates containing the same solvent in pairs. The values of torsion angles τ_1 and τ_2 introducing the largest structure diversity are given after geometry optimization in *Quantum ESPRESSO*.

Structure	Space group	Z / Z'	Hydrogen bonding	τ_1 / °	τ_2 / °	RMSD / Å
^{B}II	*P*-1	6 / 3	$R_2^2(8)$ dimers	48.6 31.1 59.5	–78.7 –168.5 –80.2	0.936/ 1.061/ 0.846[a]
^{D}II	$P2_1/c$	4 / 1	$R_2^2(8)$ dimers	–130.8	–165.2	
^{B}DH	$P2_1/n$	4 / 1	Chains with water[b]	–109.3	–58.5	0.614
^{D}DH	$P2_1/n$	4 / 1	Chains with water[b]	–129.3	–54.1	
^{B}S$_{EtOH}$	$P2_1/c$	4 / 1	$C_2^2(10)$ w/s	–109.9	–70.4	0.655/ *0.672*[d]
^{D}S$_{EtOH}$	*P-1*	2 / 1	$R_2^2(8)$ dimers + *D* w/s[c]	–125.3 *126.7*[d]	–65.1 *64.9*[d]	
^{B}S$_{MeOH}$	$P2_1/c$	4 / 1	$C_2^2(10)$ w/s	–108.5	–71.4	0.658/ *0.662*[d]
^{D}S$_{MeOH}$	*P-1*	2 / 1	$R_2^2(8)$ dimers + *D* w/s[c]	–123.3 *125.2*[d]	–65.9 *67.0*[d]	
^{B}S$_{ACN}$	*P-1*	2 / 1	$R_2^2(8)$ dimers	–113.9	–71.9	0.831/ 0.829
^{D}S$_{ACN}$	*P1*	2 / 2	$R_2^2(8)$ dimers	–126.9 126.0	–63.6 64.1	

[a] – RMSD value for non-hydrogen atom positions for each symmetry independent benperidol molecule;

[b] – Chains are formed by hydrogen bonding in different manner, see Figure S16;

[c] – w/s = with solvent;

[d] – the value for the second symmetry independent molecule in *P1* space group as modelled in *Quantum ESPRESSO* is given in italic.

As the overall shape of the molecule is affected not only by the torsion angles τ_1 and τ_2 characterizing the arrangement of benzimidazol-2-one ring and 4-fluorophenyl-4-oxobutyl chain

with respect to the central piperidine / 1,2,3,6-tetrahydropyridine ring but also by the different geometry of the central ring and differences in other torsion angles, whole molecules were overlaid (see Table S12) and RMSD of non-hydrogen atoms were calculated, see Table 2. Although this comparison confirmed the nonsolvate pair **^{B}II - ^{D}II** to be the most different, also the solvate pairs were notably different, with dihydrates being the most similar pair.

To obtain more quantitative information on the energy penalty associated with the adaption of the conformation by the replaced molecule, conformation energy with respect to the global energy minimum was calculated using *Gaussian 09* for molecules in the original structures, for the replaced molecule in the substituted structures as well as for the molecule in the isostructural structures (see Figure 2). These calculations showed that in all of the original structures except for the **^{B}II** the conformation energy is close to that of the global energy minimum. In contrast, in most cases replacement of one or all of the molecules resulted in adoption of energetically inefficient conformation by the replaced molecule, as could be predicted by the large RMSD values between molecules in all structure pairs. The smallest energy penalty was observed for replacement of benperidol with droperidol in **^{B}II** because the original structure already has high conformation energy, and replacement of one of the molecules was even associated with energy lowering. Overall, the energy penalty for replacement of droperidol with benperidol is close to 10 kJ mol^{-1} in all of the structures, whereas replacement of benperidol with droperidol in general is associated with lower energy increase. We also observed that in some of the structures (**^{B}DH**, **^{D}DH** and **^{D}II**) there is a notable energy penalty for replacement of 1 of the 4 molecules in the unit cell, whereas a structure where all of the molecules are replaced could adopt and only a minor increase in the conformation energy is present.

Table 3. Intramolecular energy of benperidol and droperidol in original structures and energy penalty (in kJ mol^{-1}) associated with replacement of one and all molecules in the unit cell.

Structure	**^{B}II** (A)	**^{B}II** (B)	**^{B}II** (C)	**^{B}S$_{EtOH}$**	**^{B}S$_{MeOH}$**	**^{B}S$_{ACN}$**	**^{B}DH**	
	Conformation energy of benperidol / kJ mol^{-1}							
Original	+9.8	+8.3	+7.1	+1.6	+1.9	+1.6	+2.1	
	Energy penalty for replacement of benperidol with droperidol / kJ mol^{-1}							
Substituted	–5.0	+4.2	+3.8	+7.1	+6.7	+6.8	+5.9	
Isostructural	–0.4	+5.6	+5.4	+6.5	+6.1	+6.6	+0.8	
Structure	**^{D}II**	**^{D}S$_{EtOH}$** (A)	**^{D}S$_{EtOH}$** (B)	**^{D}S$_{MeOH}$** (A)	**^{D}S$_{MeOH}$** (B)	**^{D}S$_{ACN}$** (A)	**^{D}S$_{ACN}$** (B)	**^{D}DH**
	Conformation energy of droperidol / kJ mol^{-1}							
Original	+2.3	+0.3	+0.3	+0.6	+0.6	+0.2	+0.2	+1.0
	Energy penalty for replacement of droperidol with benperidol / kJ mol^{-1}							
Substituted	+9.6	+9.7	+9.8	+9.6	+8.9	+10.0	+9.9	+8.7
Isostructural	+2.4	+8.9	+8.9	+9.0	+8.9	+9.0	+8.6	+1.7

Comparison of intermolecular interaction energy

We also evaluated the changes in the intermolecular interaction energy introduced by the replacement of the molecules. Intermolecular interaction energy for all the three sets of structures were calculated using *Quantum ESPRESSO*. The obtained data are presented in Table 4. Overall, replacement of one of the molecules is always associated with energy increase, which is the smallest for **^{B}II**, **^{B}S$_{MeOH}$**, and **^{B}S$_{EtOH}$**. However, full replacement of all the benperidol molecules with droperidol results in more efficient interactions in most of the structures, with the highest decrease of interaction energy calculated for **^{B}S$_{EtOH}$**. In contrast, replacement of droperidol molecules with benperidol always results in less efficient interactions. These results confirm that the interaction energy is important factor in determining the molecule replacement capability in different structures and predict the existence of solid solution in **^{B}S$_{EtOH}$** structure, although the facile formation of **^{B}II** and the relatively narrow concentration range for **^{B}S$_{ACN}$** is not predicted by these results.

Table 4. Intermolecular interaction energy in original benperidol and droperidol crystal structures (in kJ per mole of benperidol or droperidol) and energy change when one or all molecules in the unit cell are replaced. For structures with Z'>1 the change of E_{inter} in substituted structures is the average value from structures where the symmetry different molecules were replaced.

Structure	**^{B}II**	**^{B}S$_{EtOH}$**	**^{B}S$_{MeOH}$**	**^{B}S$_{ACN}$**	**^{B}DH**
	E_{inter} of benperidol structures / kJ mol^{-1}				
Original	–244.7	–331.6	–318.2	–288.4	–404.7
	Change of E_{inter} by insertion of droperidol / kJ mol^{-1}				
Substituted	+2.9	+3.6	+3.0	+5.2	+7.8
Isostructural	–0.7	–5.4	–1.8	–3.6	+5.4
Structure	**^{D}II**	**^{D}S$_{EtOH}$**	**^{D}S$_{MeOH}$**	**^{D}S$_{ACN}$**	**^{D}DH**
	E_{inter} of droperidol structures / kJ mol^{-1}				
Original	–237.3	–284.4	–281.0	–275.3	–403.5
	Change of E_{inter} by insertion of benperidol / kJ mol^{-1}				
Substituted	+5.4	+5.5	+6.3	+4.4	+4.2
Isostructural	+5.3	+7.4	+8.0	+7.6	+9.6

To identify the cause of the observed change of intermolecular interaction energy by molecule replacement we also calculated pairwise intermolecular interaction energies for the closest molecules for all three sets of structures in *CrystalExplorer*. Firstly, we evaluated the effect of molecule replacement on the hydrogen bond interaction strength, see Table S23. Overall, we see that the hydrogen bond interactions do not restrict the formation of solid solutions, as for the nonsolvate and solvate structures with $R_2^2(8)$ dimers mostly no noticeable changes are introduced by the molecule replacement. The largest changes for dimers (+2 - +3 kJ mol^{-1}) were introduced by inserting benperidol molecule in **^{D}II**, which nevertheless agrees with solid solution never observed in this structure. Generally, larger changes were introduced for hydrogen bonds formed with solvent molecules, with changes up to +3 - +5 kJ mol^{-1} for **^{D}S$_{EtOH}$**, **^{D}S$_{MeOH}$**, and **^{D}DH**, and up

to +2 - +3 kJ mol^{-1} for benperidol solvates. In benperidol solvates, however, no correlation with the ability of structure to form solid solution was observed.

Secondly, we evaluated the effect of molecule replacement on the interaction energy for molecule pairs forming the strongest dispersion interactions (for molecule pairs with E_{disp} < –45 kJ mol^{-1}, corresponding to 3 – 6 interactions for each benperidol / droperidol molecule depending on the structure), see Table 5 and Table S24. Although, overall, no critical differences in such interactions were introduced by molecule replacement, average interaction energy for such pairs became less efficient by ~2 kJ mol^{-1} for droperidol solvates ^{D}**S**$_{EtOH}$, ^{D}**S**$_{MeOH}$, and ^{D}**S**$_{ACN}$ and by 3 - 4 kJ mol^{-1} for ^{D}**II** and ^{B}**DH**. In contrast, the average interaction energy for such pairs almost did not change for ^{D}**DH**, ^{B}**II** and ^{B}**S**$_{MeOH}$, and became more efficient by ~1 kJ mol^{-1} for benperidol solvates ^{B}**S**$_{EtOH}$ and ^{B}**S**$_{ACN}$. We note that for more than half of the analyzed structures the energy change appearing in the substituted structure was magnified in the isostructural structure. In contrast, the total intermolecular interaction energy values (Table 4) in the substituted structures were always calculated to be less efficient than in the original structures.

Table 5. The relative average intermolecular interaction energy (in kJ mol^{-1}) with respect to that in the original structures for molecule pairs forming the strongest dispersion interactions.

Structure	^{B}**II**	^{B}**S**$_{EtOH}$	^{B}**S**$_{MeOH}$	^{B}**S**$_{ACN}$	^{B}**DH**
Substituted	+0.6	–0.7	+0.6	+0.4	+2.1
Isostructural	–0.2	–1.0	–0.1	–0.6	+3.6
Structure	^{D}**II**	^{D}**S**$_{EtOH}$	^{D}**S**$_{MeOH}$	^{D}**S**$_{ACN}$	^{D}**DH**
Substituted	+1.5	+0.5	+0.8	+0.4	–0.1
Isostructural	+2.6	+1.9	+1.8	+2.0	0.0

We see that overall, there is a correlation between the ability of a structure to form a solid solution and the total interaction energy of structure as well as the interaction energy for molecule pairs forming the strongest dispersion interactions. In contrast, analysis of just hydrogen bond

interactions do not provide information on the ability of structures to form solid solutions. The interaction energy analysis, however, do not explain the rather poor solid solution formation in **$^{B}S_{ACN}$** structures, the average solid solution formation in **^{B}DH** structure, and the very good solid solution formation of **^{B}II**.

Thirdly, we present more comprehensive view on the energy differences by analyzing the interaction energy for all molecule pairs formed by molecules for which atoms within 3.80 Å radius from the central molecule are present (Tables S13 – S22). Using these values, we calculated cumulative interaction energy from the molecule pairs with increasing distance between molecular centroids and plotted the difference between this energy in substituted and isostructural structures and that in the original structure. Selected plots are given in Figure 6, and the remaining plots in Figure S20.

From these plots it can clearly be seen that the only structure with more efficient cumulative interaction energy from all such molecule pairs in both substituted and isostructural structures is **$^{B}S_{EtOH}$** easily forming solid solution. Although the cumulative energy for isostructural structures were also favorable for **$^{B}S_{MeOH}$** and **$^{B}S_{ACN}$**, the limited solid solution formation by these structures could be explained by the inefficient energy for substituted structures. Likewise, similar trends for the cumulative energy were present also for **^{B}II**, confirming that overall formation of solid solutions in this structure is highly likely. Generally, molecule replacement reduced efficiency of interactions in droperidol solvates **$^{D}S_{EtOH}$**, **$^{D}S_{MeOH}$**, and **$^{D}S_{ACN}$**, whereas no significant effect on **^{D}DH** was introduced. Clearly in **^{D}II** the interactions experience the most notable efficiency loss, which is consistent with this structure never being experimentally observed. Molecule replacement also significantly reduced the efficiency of interactions in **^{B}DH**, with notable energy loss observed for two identical molecule pairs where oppositely oriented piperidin-dihydrobenzimidazolone

rings interacted (also being the main contribution in increasing the average interaction energy for molecule pairs forming the strongest dispersion interactions, Table 5). Nevertheless, we believe that this could as well be caused by some problems in modelling structures of **^{B}DH**, as experimentally solid solution in this structure formed as good as in **^{B}S$_{ACN}$** and better than in **^{D}DH**.

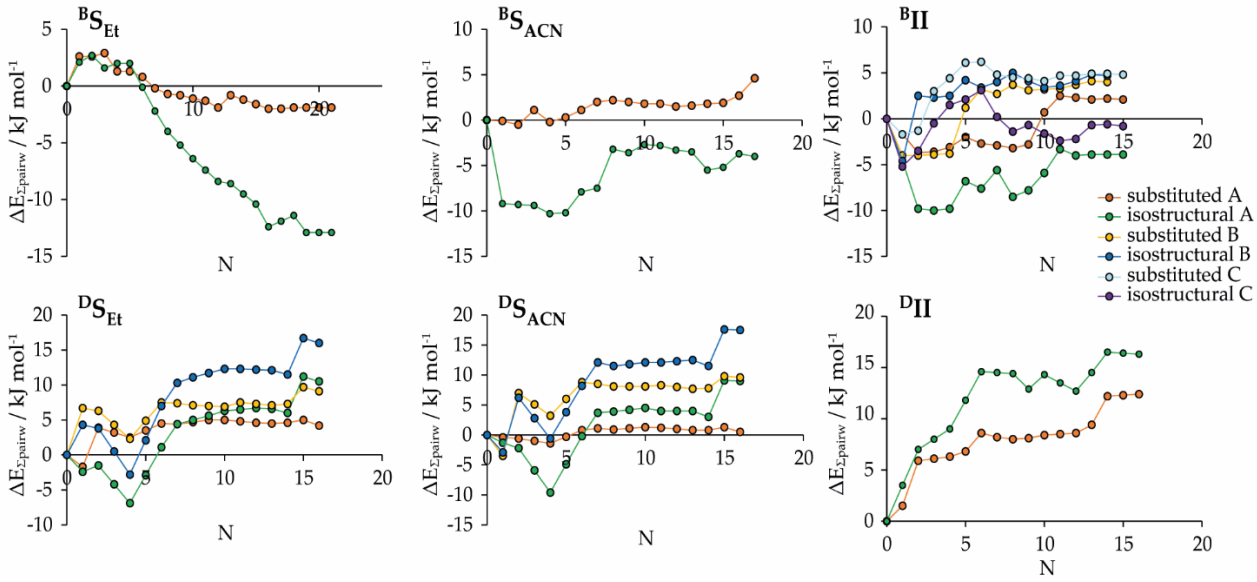

Figure 6. Difference of cumulative interaction energy from the molecule pairs with increasing distance between molecular centroids between substituted and isostructural structures and that of the original structure plotted by increasing distance (N = molecule number).

This analysis also clearly shows that interactions with the closest molecules are not the ones determining the molecule replacement ability. For example, contrary to the observed formation of solid solutions, considering only the closest 4 molecules the replacement is inefficient in **^{B}S$_{EtOH}$**, but efficient for the isostructural structure of **^{D}S$_{EtOH}$**. Note, however, that the closest molecules do not necessarily correspond to efficient intermolecular interactions, and the hydrogen bonded molecules for hydrogen bonded dimers are among the most distant molecules considered in this analysis.

Considering the differences in phase composition between the considered structures, the analysis of the intermolecular interaction energies suggest that in this system solid solutions are more easily formed in single component phases, as solid solution over wide composition range can experimentally be obtained if the molecule replacement maintains the same interaction efficiency as in the original structure, whereas for solvated phases formation of solid solution over wide composition range requires notably favorable interactions if compared to the original structure. Although this is contrary to the observation that a third component can allow the miscibility of two immiscible components in the solid state[78], in the case of solvates the solvent could complicate the miscibility in the structure if it increases the number or importance of spatially oriented interactions. Another explanation for the observed different solid solution formation behavior of the structures having similar low change of intermolecular interaction energy by molecule replacement, however, could be the different penalty associated with the adaption of the conformation, which was lower for **^{B}II** structure (only +1 kJ mol^{-1} for substituted and +3.5 kJ mol^{-1} for isostructural) if compared to that for **^{B}S$_{MeOH}$** and **^{B}S$_{ACN}$** (+7 kJ mol^{-1} for substituted and +6.5 kJ mol^{-1} for isostructural).

4. Conclusions

We show that in benperidol-droperidol system solid solutions in different crystal structures form notably differently, and the extent up to which a structure can accommodate the other molecule strongly depends on the crystal structure. There are structure pairs in which droperidol can dissolve in a benperidol crystal structure almost up to complete replacement (90% replacement was reached for **^{B}S$_{EtOH}$** and **^{B}II** structures) of benperidol molecules with droperidol molecules, whereas replacement of droperidol with benperidol in the corresponding droperidol phases was not observed. In contrast, in the other studied structure pairs (dihydrates and methanol and acetonitrile

solvates) we observe notably lower ability of droperidol to replace benperidol in benperidol structures, but in these pairs benperidol can replace droperidol in droperidol structures. Nevertheless, benperidol still cannot replace droperidol in droperidol structures up to such an extent as observed for the reverse replacement direction.

We also show that desolvation of all the solvated crystallization products obtained by crystallizing benperidol and droperidol in any ratio results in formation of pure solid solution in **^{B}II** structure regardless of the initial solvated phase composition of the sample. This means that the solid solution in this structure has a superior stability over other potential nonsolvated phases and the desolvation of all solvates occur via recrystallization of the sample and is not a simple structure rearrangement after the solvent loss.

We demonstrate that considered analysis of the interaction energy changes introduced by the replacement of molecules in each crystal structure in general allow rationalization of the solid solution formation ability by each structure. This analysis demonstrates that there is no one interaction defining whether the molecule replacement in the structure will be possible, but consideration of all the interaction energies of nearby molecules, particularly the dispersion-type interactions, allow prediction of the solid solution formation likelihood. This clearly allowed identification of **^{B}S$_{EtOH}$** as structure in which molecule replacement is the most energetically favored. Additionally, the results suggest that the formation of solid solutions in wide concentration range in nonsolvated structures require maintaining the interaction efficiency, whereas formation of solid solutions in wide concentration range in the studied solvates are more difficult and require increase of the interaction efficiency.

Associated content

Supporting Information

The Supporting Information is available free of charge on the ACS Publications website at https://pubs.acs.org/doi/10.1021/acs.cgd._____.

Additional data of crystallization experiments, solid form characterization, i.e., PXRD patterns, DSC curves and ^{1}H-NMR spectra of different composition samples, additional results and data from comparison of crystal structures and calculation of pairwise intermolecular interaction energy (PDF).

Author information

Corresponding Author

Agris Bērziņš – *Faculty of Chemistry, University of Latvia, LV-1004 Riga, Latvia; orcid.org/0000-0002-4149-8971;*

Email: agris.berzins@lu.lv

Author

Kristaps Saršūns – *Faculty of Chemistry, University of Latvia, LV-1004 Riga, Latvia; orcid.org/0000-0002-8692-7768*

Complete contact information is available at: https://pubs.acs.org/10.1021/acs.cgd._____

Notes

The authors declare no competing financial interest.

Funding

This research was funded by the MikroTik Ltd project *Development of integrated experimental and computer modelling research methodology for prediction of the properties and diversity of*

phases of active pharmaceutical solids administrated by the University of Latvia Foundation, project No. AHL-2202 and Latvian Council of Science project *Crystal engineering of pharmaceutical multicomponent phases for more efficient crystalline phase design*, project No. lzp-2018/1-0312.

Acknowledgements

KS acknowledges financial support from the European Social Fund project *Strengthening of the capacity of doctoral studies at the University of Latvia within the framework of the new doctoral model*, identification No. 8.2.2.0/20/I/006 and MikroTik Ltd. doctoral scholarship in the field of natural and medical sciences administrated by the University of Latvia Foundation. We thank Rihards Klūga (University of Latvia) for ^{1}H-NMR spectra measurements.

References

(1) Aakeröy, C. B.; Sinha, A. S. *Co-Crystals: Preparation, Characterization and Applications*; Aakeröy, C. B., Sinha, A. S., Eds.; Monographs in Supramolecular Chemistry; Royal Society of Chemistry: Cambridge, 2018; Vol. 24. https://doi.org/10.1039/9781788012874.

(2) Aakeröy, C. B.; Seddon, K. R. The Hydrogen Bond and Crystal Engineering. *Chem. Soc. Rev.* **1993**, *22* (6), 397–407. https://doi.org/10.1039/CS9932200397.

(3) Wittenberg, J. B.; Isaacs, L. Complementarity and Preorganization. *Supramol. Chem.* **2012**. https://doi.org/10.1002/9780470661345.smc004.

(4) Cavallo, G.; Metrangolo, P.; Milani, R.; Pilati, T.; Priimagi, A.; Resnati, G.; Terraneo, G. The Halogen Bond. *Chem. Rev.* **2016**, *116* (4), 2478–2601. https://doi.org/10.1021/acs.chemrev.5b00484.

(5) Mukherjee, A.; Tothadi, S.; Desiraju, G. R. Halogen Bonds in Crystal Engineering: Like Hydrogen Bonds yet Different. *Acc. Chem. Res.* **2014**, *47* (8), 2514–2524. https://doi.org/10.1021/ar5001555.

(6) Galek, P. T. A.; Fábián, L.; Motherwell, W. D. S.; Allen, F. H.; Feeder, N. Knowledge-Based Model of Hydrogen-Bonding Propensity in Organic Crystals. *Acta Crystallogr. Sect. B Struct. Sci.* **2007**, *63* (5), 768–782. https://doi.org/10.1107/S0108768107030996.

(7) Wood, P. A.; Feeder, N.; Furlow, M.; Galek, P. T. A.; Groom, C. R.; Pidcock, E. Knowledge-Based Approaches to Co-Crystal Design. *CrystEngComm* **2014**, *16* (26), 5839–5848. https://doi.org/10.1039/c4ce00316k.

(8) Sarkar, N.; Sinha, A. S.; Aakeroÿ, C. B. Systematic Investigation of Hydrogen-Bond Propensities for Informing Co-Crystal Design and Assembly. *CrystEngComm* **2019**, *21* (40), 6048–6055. https://doi.org/10.1039/c9ce01196j.

(9) Wood, P. A.; Olsson, T. S. G.; Cole, J. C.; Cottrell, S. J.; Feeder, N.; Galek, P. T. A.; Groom,

C. R.; Pidcock, E. Evaluation of Molecular Crystal Structures Using Full Interaction Maps. *CrystEngComm* **2013**, *15* (1), 65–72. https://doi.org/10.1039/c2ce25849h.
(10) Devogelaer, J. J.; Meekes, H.; Vlieg, E.; de Gelder, R. Cocrystals in the Cambridge Structural Database: A Network Approach. *Acta Crystallogr. Sect. B Struct. Sci. Cryst. Eng. Mater.* **2019**, *75*, 371–383. https://doi.org/10.1107/S2052520619004694.
(11) Takieddin, K.; Khimyak, Y. Z.; Fábián, L. Prediction of Hydrate and Solvate Formation Using Statistical Models. *Cryst. Growth Des.* **2016**, *16* (1), 70–81. https://doi.org/10.1021/acs.cgd.5b00966.
(12) Xin, D.; Gonnella, N. C.; He, X.; Horspool, K. Solvate Prediction for Pharmaceutical Organic Molecules with Machine Learning. *Cryst. Growth Des.* **2019**, *19* (3), 1903–1911. https://doi.org/10.1021/acs.cgd.8b01883.
(13) Vriza, A.; Sovago, I.; Widdowson, D.; Kurlin, V.; Wood, P. A.; Dyer, M. S. Molecular Set Transformer: Attending to the Co-Crystals in the Cambridge Structural Database. *Digit. Discov.* **2022**. https://doi.org/10.1039/d2dd00068g.
(14) Musumeci, D.; Hunter, C. A.; Prohens, R.; Scuderi, S.; McCabe, J. F. Virtual Cocrystal Screening. *Chem. Sci.* **2011**, *2* (5), 883–890. https://doi.org/10.1039/c0sc00555j.
(15) Chan, H. C. S.; Kendrick, J.; Neumann, M. A.; Leusen, F. J. J. Towards Ab Initio Screening of Co-Crystal Formation through Lattice Energy Calculations and Crystal Structure Prediction of Nicotinamide, Isonicotinamide, Picolinamide and Paracetamol Multi-Component Crystals. *CrystEngComm* **2013**, *15* (19), 3799–3807. https://doi.org/10.1039/c3ce40107c.
(16) Shishkin, O. V.; Zubatyuk, R. I.; Shishkina, S. V.; Dyakonenko, V. V.; Medviediev, V. V. Role of Supramolecular Synthons in the Formation of the Supramolecular Architecture of Molecular Crystals Revisited from an Energetic Viewpoint. *Phys. Chem. Chem. Phys.* **2014**, *16* (14), 6773. https://doi.org/10.1039/c3cp55390f.
(17) Price, S. L. Control and Prediction of the Organic Solid State: A Challenge to Theory and Experiment. *Proc. R. Soc. A Math. Phys. Eng. Sci.* **2018**, *474* (2217). https://doi.org/10.1098/rspa.2018.0351.
(18) Price, S. L.; Reutzel-Edens, S. M. The Potential of Computed Crystal Energy Landscapes to Aid Solid-Form Development. *Drug Discov. Today* **2016**, *21* (6), 912–923. https://doi.org/10.1016/j.drudis.2016.01.014.
(19) Nyman, J.; Reutzel-Edens, S. M. Crystal Structure Prediction Is Changing from Basic Science to Applied Technology. *Faraday Discuss.* **2018**, *211*, 459–476. https://doi.org/10.1039/c8fd00033f.
(20) Blagden, N.; de Matas, M.; Gavan, P. T.; York, P. Crystal Engineering of Active Pharmaceutical Ingredients to Improve Solubility and Dissolution Rates. *Adv. Drug Deliv. Rev.* **2007**, *59* (7), 617–630. https://doi.org/10.1016/j.addr.2007.05.011.
(21) Sandhu, B.; Sinha, A. S.; Desper, J.; Aakeröy, C. B. Modulating the Physical Properties of Solid Forms of Urea Using Co-Crystallization Technology. *Chem. Commun.* **2018**, *54* (37), 4657–4660. https://doi.org/10.1039/c8cc01144c.
(22) Garain, S.; Ansari, S. N.; Kongasseri, A. A.; Chandra Garain, B.; Pati, S. K.; George, S. J. Room Temperature Charge-Transfer Phosphorescence from Organic Donor-Acceptor Co-Crystals. *Chem. Sci.* **2022**, *13* (34), 10011–10019. https://doi.org/10.1039/d2sc03343g.
(23) Saha, S.; Mishra, M. K.; Reddy, C. M.; Desiraju, G. R. From Molecules to Interactions to Crystal Engineering: Mechanical Properties of Organic Solids. *Acc. Chem. Res.* **2018**, *51* (11), 2957–2967. https://doi.org/10.1021/acs.accounts.8b00425.

(24) Perlovich, G. Melting Points of One- and Two-Component Molecular Crystals as Effective Characteristics for Rational Design of Pharmaceutical Systems. *Acta Crystallogr. B. Struct. Sci. Cryst. Eng. Mater.* **2020**, *76* (February), 696–706. https://doi.org/10.1107/S2052520620007362.
(25) Krueger, E. L.; Sinha, A. S.; Desper, J.; Aakeröy, C. B. Exploring Binding Preferences in Co-Crystals of Conformationally Flexible Multitopic Ligands. *CrystEngComm* **2017**, *19* (31), 4605–4614. https://doi.org/10.1039/c7ce01177f.
(26) Aitipamula, S.; Mapp, L. K.; Wong, A. B. H.; Chow, P. S.; Tan, R. B. H. Novel Pharmaceutical Cocrystals of Triflusal: Crystal Engineering and Physicochemical Characterization. *CrystEngComm* **2015**, *17* (48), 9323–9335. https://doi.org/10.1039/c5ce01756d.
(27) Gunawardana, C. A.; Aakeröy, C. B. Co-Crystal Synthesis: Fact, Fancy, and Great Expectations. *Chem. Commun.* **2018**, *54* (100), 14047–14060. https://doi.org/10.1039/c8cc08135b.
(28) Aakeröy, C. B.; Wijethunga, T. K.; Desper, J. Molecular Electrostatic Potential Dependent Selectivity of Hydrogen Bonding. *New J. Chem.* **2015**, *39* (2), 822–828. https://doi.org/10.1039/c4nj01324g.
(29) Corpinot, M. K.; Bučar, D.-K. A Practical Guide to the Design of Molecular Crystals. *Cryst. Growth Des.* **2019**, *19* (2), 1426–1453. https://doi.org/10.1021/acs.cgd.8b00972.
(30) Corpinot, M. K.; Stratford, S. A.; Arhangelskis, M.; Anka-Lufford, J.; Halasz, I.; Judaš, N.; Jones, W.; Bučar, D. K. On the Predictability of Supramolecular Interactions in Molecular Cocrystals-the View from the Bench. *CrystEngComm* **2016**, *18* (29), 5434–5439. https://doi.org/10.1039/c6ce00293e.
(31) Desiraju, G. R. The C-H...O Hydrogen Bond: Structural Implications and Supramolecular Design. **1996**, *29*, 441–449.
(32) Taylor, R. It Isn't, It Is: The C-H···X (X = O, N, F, Cl) Interaction Really Is Significant in Crystal Packing. *Cryst. Growth Des.* **2016**, *16* (8), 4165–4168. https://doi.org/10.1021/acs.cgd.6b00736.
(33) Gavezzotti, A.; Presti, L. Lo. Building Blocks of Crystal Engineering: A Large-Database Study of the Intermolecular Approach between C-H Donor Groups and O, N, Cl, or F Acceptors in Organic Crystals. *Cryst. Growth Des.* **2016**, *16* (5), 2952–2962. https://doi.org/10.1021/acs.cgd.6b00305.
(34) Yu, L.; Stephenson, G. A.; Mitchell, C. A.; Bunnell, C. A.; Snorek, S. V.; Bowyer, J. J.; Borchardt, T. B.; Stowell, J. G.; Byrn, S. R. Thermochemistry and Conformational Polymorphism of a Hexamorphic Crystal System. *J. Am. Chem. Soc.* **2000**, *122* (4), 585–591. https://doi.org/10.1021/ja9930622.
(35) López-Mejías, V.; Kampf, J. W.; Matzger, A. J. Nonamorphism in Flufenamic Acid and a New Record for a Polymorphic Compound with Solved Structures. *J. Am. Chem. Soc.* **2012**, *134* (24), 9872–9875. https://doi.org/10.1021/ja302601f.
(36) Bhowal, R.; Chopra, D. Investigating the Role of Weak Interactions to Explore the Polymorphic Diversity in Difluorinated Isomeric N-Phenylcinnamamides. *Cryst. Growth Des.* **2021**, *21* (7), 4162–4177. https://doi.org/10.1021/acs.cgd.1c00422.
(37) Berziņš, A.; Zvaniņa, D.; Trimdale, A. Detailed Analysis of Packing Efficiency Allows Rationalization of Solvate Formation Propensity for Selected Structurally Similar Organic Molecules. *Cryst. Growth Des.* **2018**, *18* (4), 2040–2045. https://doi.org/10.1021/acs.cgd.7b01457.

(38) Bērziņš, A.; Kons, A.; Saršūns, K.; Belyakov, S.; Actiņš, A. On the Rationalization of Formation of Solvates: Experimental and Computational Study of Solid Forms of Several Nitrobenzoic Acid Derivatives. *Cryst. Growth Des.* **2020**, *20* (9), 5767–5784. https://doi.org/10.1021/acs.cgd.0c00331.
(39) Trimdale, A.; Mishnev, A.; Bērziņš, A. Combined Use of Structure Analysis, Studies of Molecular Association in Solution, and Molecular Modelling to Understand the Different Propensities of Dihydroxybenzoic Acids to Form Solid Phases. *Pharmaceutics* **2021**, *13* (5), 734. https://doi.org/10.3390/pharmaceutics13050734.
(40) Price, C. P.; Glick, G. D.; Matzger, A. J. Dissecting the Behavior of a Promiscuous Solvate Former. *Angew. Chemie - Int. Ed.* **2006**, *45* (13), 2062–2066. https://doi.org/10.1002/anie.200503533.
(41) Boothroyd, S.; Kerridge, A.; Broo, A.; Buttar, D.; Anwar, J. Why Do Some Molecules Form Hydrates or Solvates? *Cryst. Growth Des.* **2018**, *18* (3), 1903–1908. https://doi.org/10.1021/acs.cgd.8b00160.
(42) Braun, D. E.; Karamertzanis, P. G.; Price, S. L. Which, If Any, Hydrates Will Crystallise? Predicting Hydrate Formation of Two Dihydroxybenzoic Acids. *Chem. Commun.* **2011**, *47* (19), 5443–5445. https://doi.org/10.1039/C1CC10762C.
(43) Braun, D. E.; Bhardwaj, R. M.; Florence, A. J.; Tocher, D. A.; Price, S. L. Complex Polymorphic System of Gallic Acid—Five Monohydrates, Three Anhydrates, and over 20 Solvates. *Cryst. Growth Des.* **2013**, *13* (1), 19–23. https://doi.org/10.1021/cg301506x.
(44) Braun, D. E. Experimental and Computational Approaches to Rationalise Multicomponent Supramolecular Assemblies: Dapsone Monosolvates. *Phys. Chem. Chem. Phys.* **2019**, *21* (31), 17288–17305. https://doi.org/10.1039/c9cp02572c.
(45) Lusi, M. A Rough Guide to Molecular Solid Solutions: Design, Synthesis and Characterization of Mixed Crystals. *CrystEngComm* **2018**, *20* (44), 7042–7052. https://doi.org/10.1039/C8CE00691A.
(46) Braga, D.; Desiraju, G. R.; Miller, J. S.; Orpen, A. G.; Price, S. L. Innovation in Crystal Engineering. *CrystEngComm* **2002**, *4* (83), 500–509. https://doi.org/10.1039/b207466b.
(47) Sacconi, L.; Ciampolini, M.; Speroni, G. P. Structure Mimicry in Solid Solutions of 3d Metal Complexes with N-Methylsalicylaldimine (Msal-Me). *J. Am. Chem. Soc.* **1965**, *87* (14), 3102–3106. https://doi.org/10.1021/ja01092a016.
(48) Romasanta, A. K. S.; Braga, D.; Duarte, M. T.; Grepioni, F. How Similar Is Similar? Exploring the Binary and Ternary Solid Solution Landscapes of p-Methyl/Chloro/Bromo-Benzyl Alcohols. *CrystEngComm* **2017**, *19* (4), 653–660. https://doi.org/10.1039/c6ce02282k.
(49) Braga, D.; Grepioni, F.; Maini, L.; Polito, M.; Rubini, K.; Chierotti, M. R.; Gobetto, R. Hetero-Seeding and Solid Mixture to Obtain New Crystalline Forms. *Chem. - A Eur. J.* **2009**, *15* (6), 1508–1515. https://doi.org/10.1002/chem.200800381.
(50) Jones, W.; Theocharis, C. R.; Thomas, J. M.; Desiraju, G. R. Structural Mimicry and the Photoreactivity of Organic Solids. *J. Chem. Soc. Chem. Commun.* **1983**, No. 23, 1443. https://doi.org/10.1039/c39830001443.
(51) Kitaigorodskii, A. I. Molecular Crystals and Molecules. *Acad. Press. New York*, **1973**, 570. https://doi.org/10.1016/0025-5408(74)90199-8.
(52) Kitaigorodskii, A. I. Conditions of Formation of Substitutional Organic Solid Solutions. In Mixed Crystals. In *Springer-Verlag: Berlin*; 1984; pp 200–216. https://doi.org/10.1007/978-3-642-81347-4_18.

(53) Corpinot, M. K.; Guo, R.; Tocher, D. A.; Buanz, A. B. M.; Gaisford, S.; Price, S. L.; Bučar, D. K. Are Oxygen and Sulfur Atoms Structurally Equivalent in Organic Crystals? *Cryst. Growth Des.* **2017**, *17* (2), 827–833. https://doi.org/10.1021/acs.cgd.6b01669.
(54) Desiraju, G. R.; Sarma, J. A. R. P. The Chloro-Methyl Exchange Rule and Its Violations in the Packing of Organic Molecular Solids. *J. Chem. Sci.* **1986**, *96* (6), 599–605. https://doi.org/10.1007/BF02936309.
(55) Saršūns, K.; Bērziņš, A.; Rekis, T. Solid Solutions in the Xanthone–Thioxanthone Binary System: How Well Are Similar Molecules Discriminated in the Solid State? *Cryst. Growth Des.* **2020**, *20* (12), 7997–8004. https://doi.org/10.1021/acs.cgd.0c01241.
(56) Mazzeo, P. P.; Carraro, C.; Arns, A.; Pelagatti, P.; Bacchi, A. Diversity through Similarity: A World of Polymorphs, Solid Solutions, and Cocrystals in a Vial of 4,4′-Diazopyridine. *Cryst. Growth Des.* **2020**, *20* (2), 636–644. https://doi.org/10.1021/acs.cgd.9b01052.
(57) Berziņš, A.; Actiņš, A. Why Do Chemically Similar Pharmaceutical Molecules Crystallize in Different Structures: A Case of Droperidol and Benperidol. *Cryst. Growth Des.* **2016**, *16* (3), 1643–1653. https://doi.org/10.1021/acs.cgd.5b01736.
(58) Fonseca, J. D. C.; Tenorio Clavijo, J. C.; Alvarez, N.; Ellena, J.; Ayala, A. P. Novel Solid Solution of the Antiretroviral Drugs Lamivudine and Emtricitabine. *Cryst. Growth Des.* **2018**, *18* (6), 3441–3448. https://doi.org/10.1021/acs.cgd.8b00164.
(59) Case, D. H.; Srirambhatla, V. K.; Guo, R.; Watson, R. E.; Price, L. S.; Polyzois, H.; Cockcroft, J. K.; Florence, A. J.; Tocher, D. A.; Price, S. L. Successful Computationally Directed Templating of Metastable Pharmaceutical Polymorphs. *Cryst. Growth Des.* **2018**, *18* (9), 5322–5331. https://doi.org/10.1021/acs.cgd.8b00765.
(60) Braga, D. Crystal Engineering, Where from? Where To? *Chem. Commun.* **2003**, *3* (22), 2751–2754. https://doi.org/10.1039/b306269b.
(61) Lusi, M. Engineering Crystal Properties through Solid Solutions. *Cryst. Growth Des.* **2018**, *18* (6), 3704–3712. https://doi.org/10.1021/acs.cgd.7b01643.
(62) Goldberg, A. H.; Gibaldi, M.; Kanig, J. L. Increasing Dissolution Rates and Gastrointestinal Absorption of Drugs via Solid Solutions and Eutectic Mixtures III: Experimental Evaluation of Griseofulvin—Succinic Acid Solid Solution. *J. Pharm. Sci.* **1966**, *55* (5), 487–492. https://doi.org/10.1002/jps.2600550508.
(63) Trotta, J. T.; Zeidan, T. A.; Tilak, P. A.; Foxman, B. M.; Almarsson, Ö.; Oliveira, M. A.; Chiarella, R. A.; Hickey, M. B.; Remenar, J. F. Aripiprazole and Dehydro-Aripiprazole Solid Solutions: Crystalline Combinations of Drug and Active Metabolite in Tailored Compositions. *Cryst. Growth Des.* **2020**, *20* (6), 3944–3956. https://doi.org/10.1021/acs.cgd.0c00263.
(64) Saršūns, K.; Kemere, M.; Karziņins, A.; Kļimenkovs, I.; Bē Rziņš, A.; Sarakovskis, A.; Rekis, T. Fine-Tuning Solid State Luminescence Properties of Organic Crystals via Solid Solution Formation: The Example of 4-Iodothioxanthone-4-Chlorothioxanthone System. *Cryst. Growth Des.* **2022**, *22* (8), 4838–4844. https://doi.org/10.1021/acs.cgd.2c00313.
(65) Weerasekara, R. K.; Uekusa, H.; Hettiarachchi, C. V. Multicolor Photochromism of Fulgide Mixed Crystals with Enhanced Fatigue Resistance. *Cryst. Growth Des.* **2017**, *17* (6), 3040–3047. https://doi.org/10.1021/acs.cgd.6b01708.
(66) Berziņš, A.; Skarbulis, E.; Rekis, T.; Actiņš, A. On the Formation of Droperidol Solvates: Characterization of Structure and Properties. *Cryst. Growth Des.* **2014**, *14* (5), 2654–2664. https://doi.org/10.1021/cg5003447.
(67) Saršūns, K.; Bērziņš, A. Prediction of Solid Solution Formation among Chemically Similar

Molecules Using Calculation of Lattice and Intermolecular Interaction Energy. *Key Eng. Mater.* **2020**, *850*, 54–59. https://doi.org/10.4028/www.scientific.net/KEM.850.54.

(68) Actins, A.; Arajs, R.; Belakovs, S.; Orola, L.; Veidis, M. V. The Crystal and Molecular Structure of a Polymorph and a Pseudo-Polymorph of Droperidol. *J. Chem. Crystallogr.* **2008**, *38* (3), 169–174. https://doi.org/10.1007/s10870-007-9283-9.

(69) Blaton, N. M.; Peeters, O. M.; De Ranter, C. J. 1-{1-[4-(4-Fluorophenyl)-4-Oxobutyl]-1,2,3,6-Tetrahydro-4-Pyridyl}-1,3-Dihydro-2 H -Benzimidazol-2-One Dihydrate (Dehydrobenzperidol®). *Acta Crystallogr. Sect. B Struct. Crystallogr. Cryst. Chem.* **1980**, *36* (11), 2828–2830. https://doi.org/10.1107/S0567740880010199.

(70) Bērziņš, A.; Skarbulis, E.; Actiņš, A. Structural Characterization and Rationalization of Formation, Stability, and Transformations of Benperidol Solvates. *Cryst. Growth Des.* **2015**, *15* (5), 2337–2351. https://doi.org/10.1021/acs.cgd.5b00138.

(71) Giannozzi, P.; Baroni, S.; Bonini, N.; Calandra, M.; Car, R.; Cavazzoni, C.; Ceresoli, D.; Chiarotti, G. L.; Cococcioni, M.; Dabo, I.; Dal Corso, A.; De Gironcoli, S.; Fabris, S.; Fratesi, G.; Gebauer, R.; Gerstmann, U.; Gougoussis, C.; Kokalj, A.; Lazzeri, M.; Martin-Samos, L.; Marzari, N.; Mauri, F.; Mazzarello, R.; Paolini, S.; Pasquarello, A.; Paulatto, L.; Sbraccia, C.; Scandolo, S.; Sclauzero, G.; Seitsonen, A. P.; Smogunov, A.; Umari, P.; Wentzcovitch, R. M. QUANTUM ESPRESSO: A Modular and Open-Source Software Project for Quantum Simulations of Materials. *J. Phys. Condens. Matter* **2009**, *21* (39). https://doi.org/10.1088/0953-8984/21/39/395502.

(72) Grimme, S. Semiempirical GGA-Type Density Functional Constructed with a Long-Range Dispersion Correction. *J. Comput. Chem.* **2006**, *27* (15), 1787–1799. https://doi.org/10.1002/jcc.20495.

(73) Lund, A. M.; Orendt, A. M.; Pagola, G. I.; Ferraro, M. B.; Facelli, J. C. Optimization of Crystal Structures of Archetypical Pharmaceutical Compounds: A Plane-Wave DFT-D Study Using Quantum Espresso. *Cryst. Growth Des.* **2013**, *13* (5), 2181–2189. https://doi.org/10.1021/cg4002797.

(74) Frisch, M. J.; Trucks, G. W.; Schlegel, H. B.; Scuseria, G. E.; Robb, M. A. . C.; J. R.; Scalmani, G.; Barone, V.; Mennucci, B.; Petersson, G. A.; Nakatsuji, H.; Caricato, M. . L.; X.; Hratchian, H. P.; Izmaylov, A. F.; Bloino, J.; Zheng, G.; Sonnenberg, J. L.; Hada, M. . E.; M.; Toyota, K.; Fukuda, R.; Hasegawa, J.; Ishida, M.; Nakajima, T.; Honda, Y.; Kitao, O. . N.; H.; Vreven, T.; Montgomery, J. A. J.; Peralta, J. E.; Ogliaro, F.; Bearpark, M.; Heyd, J. J. .; Brothers, E.; Kudin, K. N.; Staroverov, V. N.; Kobayashi, R.; Normand, J.; Raghavachari, K. .; Rendell, A.; Burant, J. C.; Iyengar, S. S.; Tomasi, J.; Cossi, M.; Rega, N.; Millam, J. M. . K.; M.; Knox, J. E.; Cross, J. B.; Bakken, V.; Adamo, C.; Jaramillo, J.; Gomperts, R. . S.; R. E.; Yazyev, O.; Austin, A. J.; Cammi, R.; Pomelli, C.; Ochterski, J. W.; Martin, R. L. .; Morokuma, K.; Zakrzewski, V. G.; Voth, G. A.; Salvador, P.; Dannenberg, J. J.; Dapprich, S. .; Daniels, A. D.; Farkas, O.; Foresman, J. B.; Ortiz, J. V.; Cioslowski, J.; Fox, D. J. *Gaussian 09, Revision D.01*; 2009.

(75) MacRae, C. F.; Sovago, I.; Cottrell, S. J.; Galek, P. T. A.; McCabe, P.; Pidcock, E.; Platings, M.; Shields, G. P.; Stevens, J. S.; Towler, M.; Wood, P. A. Mercury 4.0: From Visualization to Analysis, Design and Prediction. *J. Appl. Crystallogr.* **2020**, *53*, 226–235. https://doi.org/10.1107/S1600576719014092.

(76) Petit, S.; Coquerel, G. Mechanism of Several Solid-Solid Transformations between Dihydrated and Anhydrous Copper(II) 8-Hydroxyquinolinates. Proposition for a Unified Model for the Dehydration of Molecular Crystals. *Chem. Mater.* **1996**, *8* (9), 2247–2258.

https://doi.org/10.1021/cm9600438.
(77) Galwey, A. K. Structure and Order in Thermal Dehydrations of Crystalline Solids. *Thermochim. Acta* **2000**, *355* (1–2), 181–238. https://doi.org/10.1016/S0040-6031(00)00448-2.
(78) Lusi, M.; Vitorica-Yrezabal, I. J.; Zaworotko, M. J. Expanding the Scope of Molecular Mixed Crystals Enabled by Three Component Solid Solutions. *Cryst. Growth Des.* **2015**, *15* (8), 4098–4103. https://doi.org/10.1021/acs.cgd.5b00685.

FOR TABLE OF CONTENTS USE ONLY

Experimental and computational investigation of benperidol and droperidol solid solutions in different crystal structures

Kristaps Saršūns and Agris Bērziņš

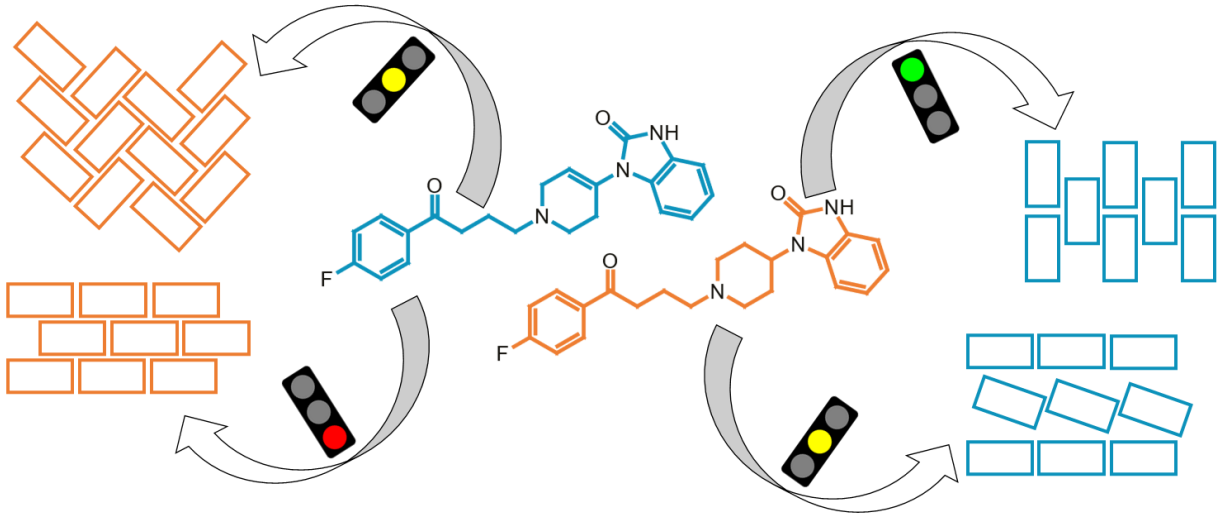

Synopsis

We explored solid solution formation between structurally highly similar active pharmaceutical ingredients droperidol and benperidol in different crystal phases and demonstrate that the formation of solid solutions strongly depends on the crystal structure. We used computational calculations to investigate the energy changes introduced by the molecule replacement and show that analysis of intermolecular interactions allows prediction of solid solution formation.

* Correspondence: agris.berzins@lu.lv; Tel.: +371-67672576